Study on k-ω shear stress transport model corrections applied to rough wall turbulent hypersonic boundary layers

M. Olazabal-Loumé[*], F. Danvin[*], J. Mathiaud[*], B. Aupoix[**]
* CEA-CESTA

15 avenue des Sablières, CS 60001 33116 Le Barp Cedex, France

*** ONERA Toulouse*
BP74025, F-31055 Toulouse France

Abstract

This work presents the application of k-ω SST model corrections [B. Aupoix, J. Fluids Engineering **137** / 021202, 2015; B. Aupoix, Int. J. Heat and Fluid Flow **56**, 160-171, 2015] to hypersonic turbulent flows. Both dynamic and thermal contributions are implemented in a Navier-Stokes code. The model verification is based on systematic comparisons with the boundary layer code CLICET. A flat plate test-case at Mach 8 is used for this purpose. Simulations of a slender cone experiment at Mach 10 [J.A.F. Hill, R.L.P. Voisinet, and D.A. Wagner, In AIAA, Aerospace Sciences Meeting, 18th, Pasadena, California, 1980] are performed as the first validation step of the model for hypersonic flows.

Nomenclature

u	velocity
ρ	density
p	pressure
T	temperature
k	turbulent kinetic energy
ω	specific dissipation rate
τ_w	wall shear stress
λ	thermal conductivity
ν	kinematic viscosity
μ	dynamic viscosity $\mu = \rho\nu$
δ	boundary layer thickness
x	longitudinal coordinate (wall frame)
y	wall normal coordinate
k_s	equivalent sand grain height
h	roughness height
S$_{corr}$	corrected wetted surface ratio
St	Stanton number
Φ	heat flux
Pr	Prandlt number

Subscripts/Superscripts

∞	freestream value
+	wall unit value
e	boundary layer outer edge value
w	wall value
r	recovery value
t	turbulent value

M. Olazabal-Loumé, F. Danvin, J. Mathiaud, B. Aupoix

1. Introduction

During a supersonic/hypersonic reentry flight, heating may damage the vehicle body causing rough surface state. In the low atmospheric layers, roughness effects on the turbulent flows have to be accounted for in CFD (Computational Fluid Dynamics) code simulations. Indeed, roughness is known to increase the skin friction and heat flux on the wall causing a dramatic modification of the aerodynamic coefficients. Usually, for such applications, turbulence effects are modeled using RANS (Reynolds Averaged Navier Stokes) approaches. Two-equation models like the k-ω Shear Stress Transport (SST) [1] model are commonly used in aeronautic applications requiring accurate treatment of the near wall turbulent flow.

For studying the roughness effect with numerical simulation, different approaches have been developed. In the direct numerical simulation (DNS), roughness elements have to be included in the initial geometry. The accuracy of the flow simulation around them and the computational cost may be prohibiting for complex and /or huge size geometries. The discrete element method consists in directly include some roughness corrective terms into the Navier-Stokes (N-S) or boundary layer equations. This method accounts for blockage effects related to the ratio between the volume accessible by the fluid over the total volume, and for form drag and heat-transfer on the roughness elements. This method has been widely used to describe the interaction between well-defined distributed roughness patterns and the turbulent flow. Nevertheless, it requires to modify the original system of equations. The equivalent sand-grain approach consists in bringing any kind of 3-D roughness to an equivalent sand-grain height to reproduce a turbulence level in the skin friction. As this method is not intrusive for an existing code, it appears to be the most suitable for industrial purposes. Several formulations were developed to be applied to RANS turbulence models. Such corrections for the k-ω SST model were recently proposed to take into account roughness effects on the skin friction and thermal flux [2-3]. They were widely validated on low Mach number experiment data. This paper presents the first application of these corrections to hypersonic flows using a Navier-Stokes code.

2. Turbulent flow modeling on a rough wall

2.1 Equivalent sand grain approach

Nikuradse's experiment study [4-5] , on the effect of distributed sand grain roughness on pressure loss in cylindrical pipes constitutes a reference work. It was observed that the roughness influence on the flow field depends on a non-dimensional sand grain height

$$k_s^+ = \frac{k_s u_\tau}{\nu_w}$$

where

$$u_\tau = \sqrt{\frac{\tau_w}{\rho}}$$

is the friction velocity.

The effect of roughness on the flow field can be decomposed into three regimes:
- Hydraulically smooth ($k_s^+ \leq 5$): The effect of roughness is not influencing the flow field. The wall skin friction remains unchanged.
- Transient ($5 \leq k_s^+ \leq 70$): Drag is generated both by viscous forces and by the pressure exerting on the roughness elements.
- Fully rough ($70 \leq k_s^+$) : Skin friction increases and the effects of roughness are independent from the Reynolds number. The viscous effects become negligible.

The given bounds can differ according to the authors. It is worth noticing that the equivalent sand-grain approach is not physical in the sense that it doesn't allow to describe the interaction between specific roughness elements and the flow. However, several correlations were proposed to calculate k_s values from real roughness geometries and enable to reproduce the effect of roughness on the skin friction.

A few years later, Schlichting [6-7] proposed for the completely rough regime to assimilate any kind of roughness to

an equivalent sand grain (of height k_s), which would generate the same skin friction increase as in Nikuradse's experiments. Importance of both roughness element form and density were pointed out. This approach is advantageous thanks to its ease of implementation and its cheap additional computational cost. Nevertheless, the method is quite sensitive to the equivalent sand-grain height estimate.

2.2 Roughness effect on the turbulent boundary layer

To study velocity variations inside the boundary layer, it is a common practice to use the non-dimensional variables u^+ and y^+ defined by

$$u^+ = \frac{u}{u_\tau}$$

$$y^+ = \frac{y\,u_\tau}{\nu_w}$$

As a reminder, skin friction and heat transfer modeling are respectively provided with a turbulent viscosity μ_t and conductivity λ_t counterpart coming from a turbulence model, thus writing

$$\tau_w = (\mu + \mu_t)\frac{\partial u}{\partial y}\Big|_w$$

and

$$\phi_w = -(\lambda + \lambda_t)\frac{\partial T}{\partial y}\Big|_w$$

It is worth reminding that a turbulent boundary layer on a smooth wall (corresponding to plain line on Figure 1) can be decomposed into three different regions [8]. In the viscous sublayer, where the viscous forces prevail due to the no-slip condition at the wall, the velocity profile can be approximated by $u^+ = y^+$ for $y^+ < 11$. Then, the log layer corresponds to a turbulence development zone with a decrease of viscous effects. The velocity profile follows the so-called logarithmic law

$$u^+ = \frac{1}{\kappa}\ln(y^+) + C$$

for $30 \leq y^+ \leq 0.1\delta$ with $\kappa = 0.41$ and $C \approx 5$. The third region is the defect layer related to the boundary layer edge state.

On a rough wall, the boundary layer structure is modified: the roughness element presence tends to suppress viscous effects in the wall vicinity. Moreover, the flow characteristics may be different above roughness elements and in the troughs between them. According to Nikuradse [4-5] and confirmed by others authors, the velocity fluctuates from the roughness trough until two to five times the actual roughness height before being able to define a mean velocity. Roughness effect is then described by introducing a ΔU^+ shift in the velocity profile logarithmic law towards lower velocities along the relation

$$u^+ = \frac{1}{\kappa}\ln(y^+) + C - \Delta U^+$$

as shown in Figure 1. Nikuradse's work also evidenced the ΔU^+ dependency regarding the non dimensional sand grain height k_s^+. Grigson's study [9] exhibited the following law on ΔU^+ in order to fit Colebrook's data [10-11]

$$\Delta U^+ = \frac{1}{\kappa}\ln\left(1 + \frac{k_s^+}{\exp[\kappa(8.5 - C)]}\right)$$

From this point, a modification of the boundary conditions of a turbulence model can be undertaken as proposed in [11].

M. Olazabal-Loumé, F. Danvin, J. Mathiaud, B. Aupoix
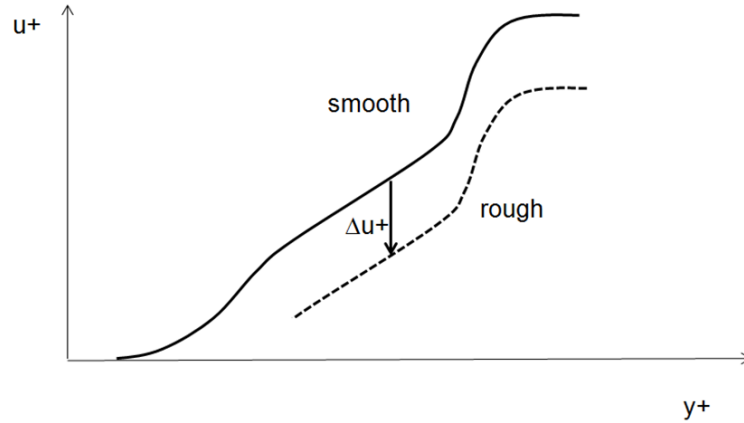
Figure 1: Turbulent boundary layer velocity profile in wall coordinates (logarithmic scale for y+). The logarithmic-law is shifted towards lower velocities due to roughness effects

3. Application to the k-ω SST turbulence model

The k-ω SST model was proposed by Menter [1] to mitigate some lack in the framework of two-equation turbulence models. It combines the suitability of Wilcox's k-ω model [12] to near wall turbulent flow capture and the k-ε model properties far from the wall. This is achieved using a coupling function F_1 so that the compressible equations of kinetic turbulent energy and specific dissipation rate conservation write respectively

$$\frac{\partial(\rho k)}{\partial t} + \frac{\partial(\rho u_j k)}{\partial x_j} = \tau_{ij}\frac{\partial u_j}{\partial x_j} - \beta^* k\omega + \frac{\partial}{\partial x_j}\left[\rho(v + \sigma_k v_T)\frac{\partial k}{\partial x_j}\right]$$

and

$$\frac{\partial(\rho\omega)}{\partial t} + \frac{\partial(\rho u_j \omega)}{\partial t} = \frac{\gamma}{v_T}\tau_{ij}\frac{\partial u_j}{\partial x_j} - \beta\omega^2 + \frac{\partial}{\partial x_j}\left[\rho(v + \sigma_\omega v_T)\frac{\partial\omega}{\partial x_j}\right] + 2(1 - F_1)\frac{\rho\sigma_{\omega_2}}{\omega}\frac{\partial k}{\partial x_j}\frac{\partial\omega}{\partial x_j}$$

where $\beta, \beta^*, \gamma, \sigma_k , \sigma_{\omega_2}$ are closure constant coefficients.

The model is completed by the kinematic viscosity limitation of the form

$$v_T = \frac{k}{\max\left(\omega, \frac{\Omega F_2}{a_1}\right)}$$

where Ω is the vorticity magnitude, a_1 a constant coefficient and F_2 a function with asymptotic behavior. Boundary conditions on a smooth wall write

$$k_w = 0, \quad \omega_w = 10\frac{6v}{\beta_1 y^2}$$

with β_1 being a constant coefficient.

3.1 Dynamic corrections

Several dynamic corrections applicable to the k-ω SST model were studied by Aupoix [2], in order to improve the predictions in the transient and fully rough regimes. ONERA-type corrections applied to Colebrook's data were selected, firstly because they overestimate the skin-friction in the transient rough regime, and secondly due to their consistency with the Von Karman's constant, which provides a fine fluid representation in the fully rough regime. These modifications applied to the k-ω SST turbulence model consist in changing the boundary conditions on k and

ω. The velocity shift is achieved thanks to an increase in the turbulence level at the wall and an increase in wall heat fluxes. From Grigson's fit on Colebrook's data, these modifications for the k- ω SST model write

$$k_w^+ = \max\left(0; k_0^+\right)$$

$$k_0^+ = \frac{1}{\sqrt{\beta^*}} tanh\left[\left(\frac{ln\frac{k_s^+}{30}}{ln\,1\,0} + 1 - tanh\frac{k_s^+}{125}\right) tanh\frac{k_s^+}{125}\right]$$

$$\omega_w^+ = \frac{300}{k_s^{+2}}\left(tanh\frac{15}{4k_s^+}\right)^{-1} + \frac{191}{k_s^+}\left(1 - exp\left(\frac{k_s^+}{250}\right)\right)$$

For applications, these values are made dimensional using the following relations

$$k_w = k_w^+ u_\tau^2$$

$$\omega_w = \omega_w^+ \frac{u_\tau^2}{\nu_w}$$

3.2 Thermal corrections

The proportional increase of wall heat fluxes with respect to drag increase, according to the Reynolds analogy, does not necessarily hold for rough walls as observed in several experiments. In ref. [3], it is suggested to account for this phenomenon by including some corrections applicable to the equivalent sand grain approach. The discrete element method was used to study different roughness element density and shape effects on heat fluxes. This database served to the construction of thermal corrections suitable to the equivalent sand grain approach to improve the wall heat flux prediction. These thermal corrections are based on a modification of the turbulent Prandtl number,

$$Pr_t = Pr_{t-Smooth} + \Delta Pr_{t-Rough}$$

in order to lower the wall heat fluxes. The turbulent Prandlt number correction depends on the equivalent sand grain height k_s, on the roughness height h, and on the corrected wetted surface ratio S_{corr}:

$$\Delta Pr_{t-Rough} = \left(A\Delta U^{+^2} + B\Delta U^+\right)exp\left(-\frac{y}{h}\right)$$

where

$$A = (0.0155 - 0.0035 S_{corr})(1 - exp[-12(S_{corr} - 1)])$$

$$B = -0.08 + 0.25 exp\left[-10(S_{corr} - 1)\right]$$

For such applications, McClain [14] defined the mean elevation as the base surface one would obtain, if the roughness elements were locally melted. From this new reference surface, only the exceeding roughness elements are taken into account to define the effective diameter d_{0eff} and height h_{eff} (see Figure 2). These results were extended to the equivalent sand grain approach and to the discrete element method. Moreover, Grigson's correlation for ΔU^+ still holds.

M. Olazabal-Loumé, F. Danvin, J. Mathiaud, B. Aupoix
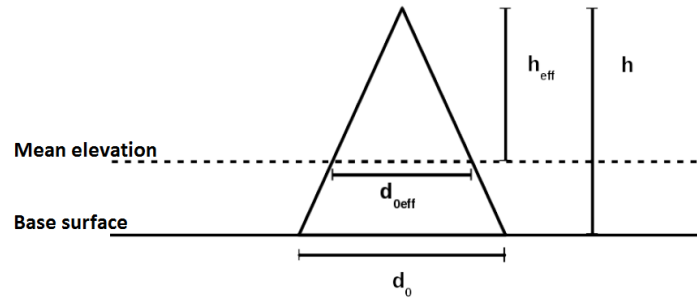
Figure 2: Mean elevation for a standard roughness element [14]
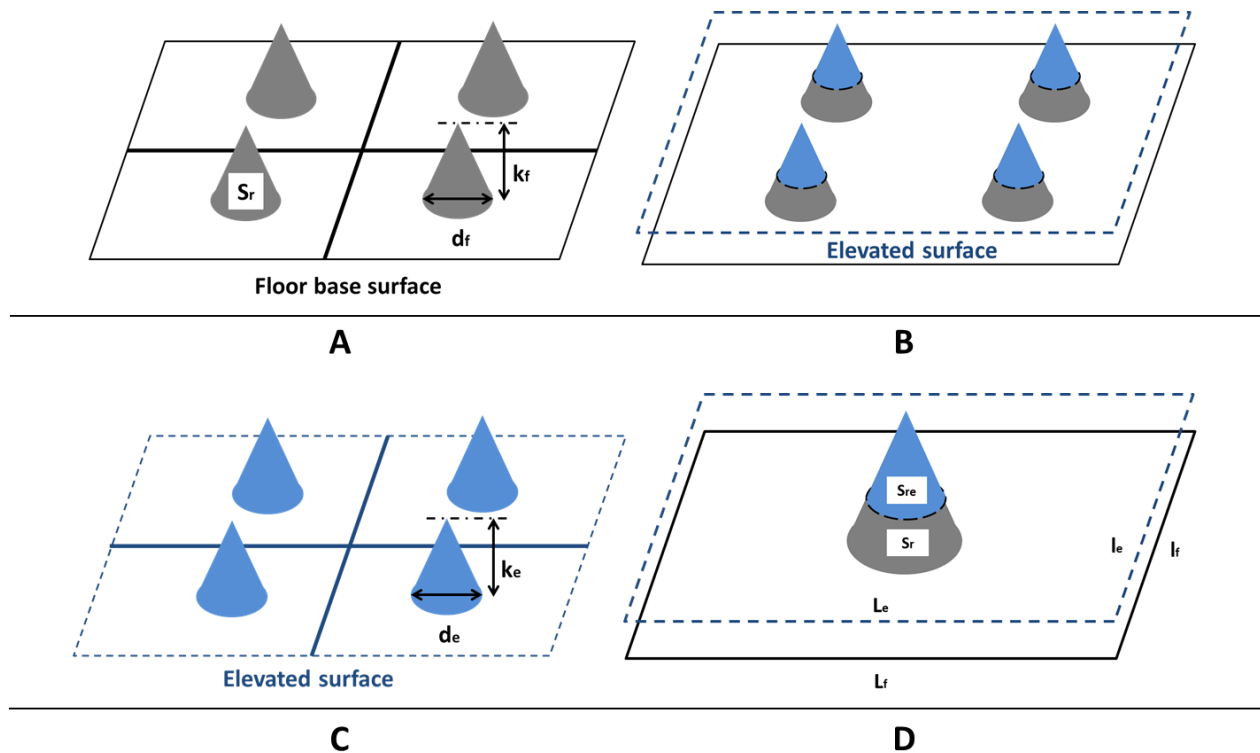
Figure 3: Process for evaluating the S_{corr} parameter

Figure 3 presents the process of evaluating the corrected wetted surface ratio S_{corr}. Considering conical roughness elements, like in McClain [14], of height k_f and base diameter d_f, one can work out the conical wetted surface S_r (subscripts "f" are associated to the floor). The second step (Fig 3-B) highlights the mean elevation described as a new base surface, obtained after melting the roughness elements (subscripts "e" are associated to this elevated surface). From this elevated surface are defined the effective part of the roughness elements (height k_e, base diameter d_e, wetted surface S_{re}). The third step consists in evaluating the new spacing between the roughness elements (L_e and l_e). Lastly one can evaluate the associated elevated wetted surface

$$S_{we} = L_e * l_e + S_{re} - \pi \frac{d_e^2}{4}$$

with the smooth (floor level) wetted surface

$$S_{wf} = L_f * l_f$$

to get

$$S_{corr} = \frac{S_{we}}{S_{wf}}$$

4. Verification on a flat plate at Mach 8

Both dynamic and thermal corrections [2-3] were implemented in the N-S code. A verification procedure was conducted using the boundary layer code CLICET [15] where the models were originally developed and validated on a variety of low Mach experiment data.

This test-case was initially proposed in [16] to evaluate turbulent flow methods on a smooth wall. A flat plate at Mach 8 is considered. The wall temperature is 1000 K and air free-stream conditions are $p_\infty = 12111.4 \, Pa$, $\rho_\infty = 0.194 \, kg/m^3$. A perfect gas equation of state is used. The shock wave emerging from the leading edge can induce modifications of the boundary layer outer edge conditions. As CLICET doesn't account for it, it was necessary to initialize the boundary layer code with the boundary layer outer edge conditions calculated by the N-S code. This procedure was first tested on laminar and turbulent flow fields on a smooth wall using different meshes. Figure 4 presents boundary layer velocity profiles for smooth and rough walls using different k_s values from 10^{-4} to 3×10^{-3} m. The shift in the logarithmic law is clearly seen in both N-S and CLICET code simulations. Figure 5 presents temperature profiles while heat flux at the wall are shown in Figure 6. Comparisons show a good agreement between the two codes despite the sensitivity of CLICET in slight modifications of the boundary layer edge conditions. Dynamic corrections are verified in the N-S code. Thermal corrections were found here to play a negligible role in the turbulent flow modification by roughness.
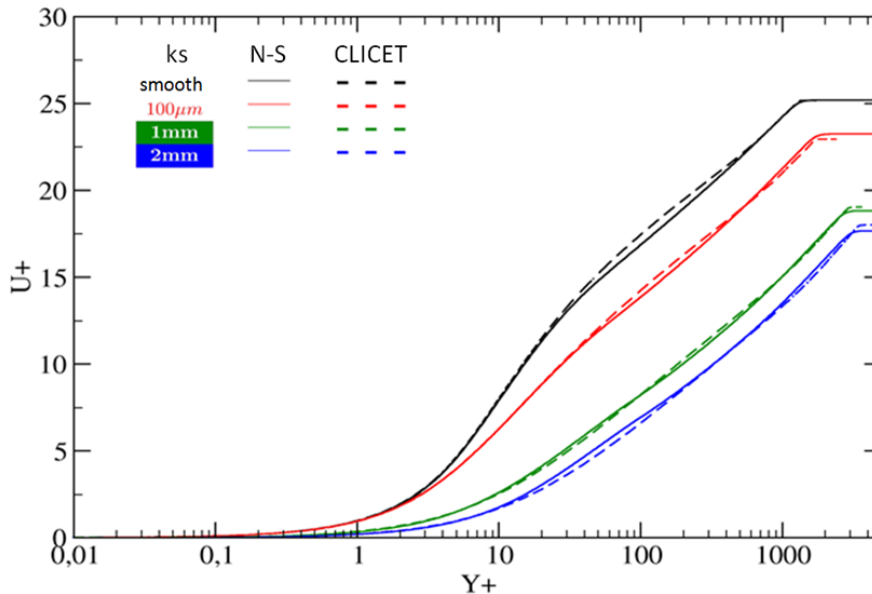
Figure 4 : Velocity profiles in the boundary layer obtained with N-S code and CLICET code for different equivalent sand grain heights

M. Olazabal-Loumé, F. Danvin, J. Mathiaud, B. Aupoix
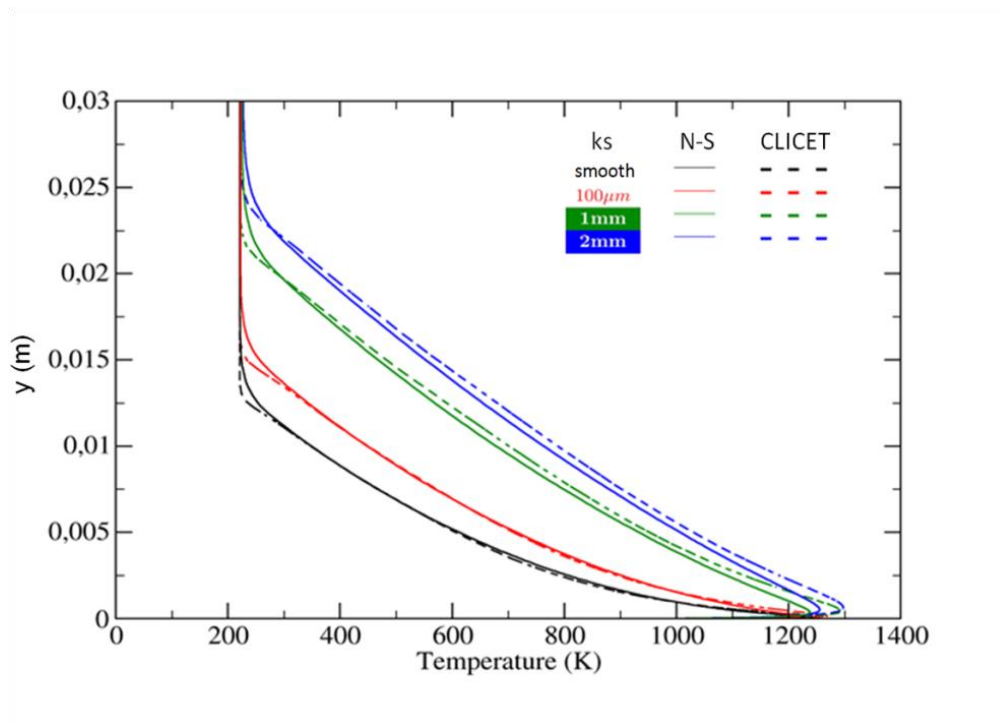
Figure 5 : Temperature profiles in the boundary layer obtained with N-S code and CLICET code for different equivalent sand grain heights
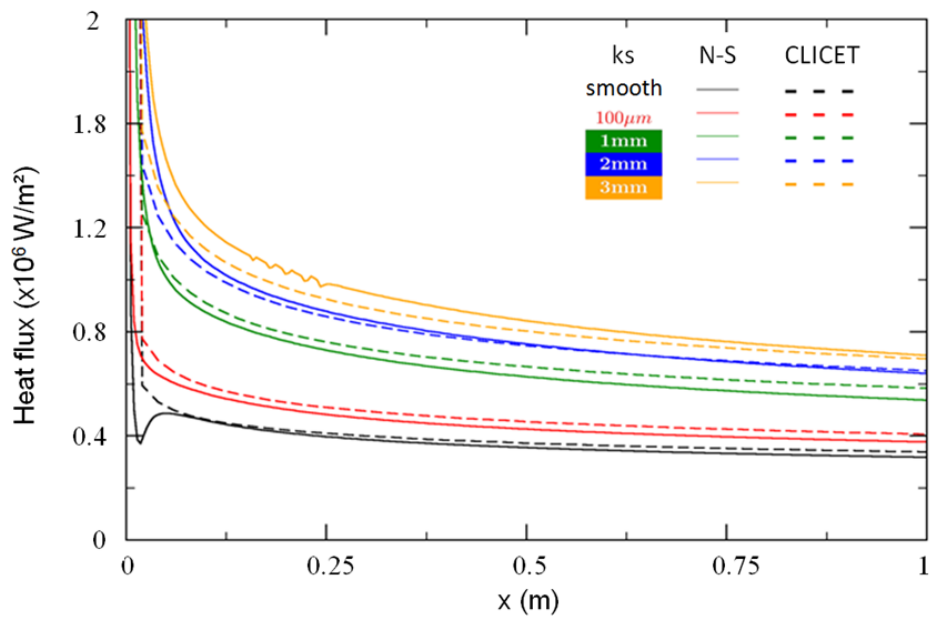
Figure 6: Heat flux on smooth and rough walls, for different equivalent sand grain heights

4. Hill experiment simulation

The paper by Hill et al. [17] reports the realization and the analysis of wind tunnel tests on a 7-degrees half-angle sharp and blunt cones at Mach 10. Nitrogen gas was used and experiment data were obtained for smooth and rough wall with three different roughness patterns. The wall temperature is 311 K. Simulations of the experiment using the N-S code and CLICET are performed for the sharp cone using the approximation of air gas and perfect gas assumption. Both dynamic and thermal corrections are used in simulations.

4.1 Equivalent sand grain height evaluation

To evaluate the equivalent sand grain height, one has to refer to Finson's study [18] where averaged roughness patterns were defined to analyse Hill's experiment data. They are based on profilometer measurements and on the assumption of identical roughness elements with uniform density to be suitable to the discrete element type method used. In the present study, due to a lack of detailed informations on the real surface state in experiment tests, these averaged roughness patterns are used to evaluate the equivalent sand grain height and the corrected wetted surface ratio needed in dynamic and thermal correction evaluations. Figure 7 presents the three different roughness element shapes while Table 1 reports the corresponding real heights h, using the following Finson's paper notations: for instance, the "11mil" case corresponds to the 11 milli-inches roughness height, i.e., 0.279×10^{-2} m in SI units. Table 1 presents also the equivalent sand grain heights k_s evaluated from Dirling's [19] and Waigh and Kind's (W-K) [20] correlations and the S_{corr} surface value. It is worth reminding that both roughness element shape and density are needed to apply such correlations. Moreover, different correlations can lead to different rough regime identification. Note also that free-stream conditions vary from one test to another and two of them correspond to smooth wall tests.

Table 1: Flow conditions and Equivalent sand grain for Finson's roughness representation with different correlations and corresponding rough regimes (HS: hydraulically smooth, TR: transient rough, FR: fully rough)

	Re_∞ $(\times 10^6)$	h $(\times 10^{-3}\,m)$	k_s (Dirling) $(\times 10^{-3}\,m)$	k_s (W-K) $(\times 10^{-3}\,m)$	S_{corr}
Smooth (1)	24.1	-	-	-	-
Smooth (2)	34.1	-	-	-	-
"11mil"	40.0	0.279	0.03229 (HS)	0.5281 (TR)	1.269
"37mil"	40.9	0.940	2.5235 (FR)	2.6381 (FR)	1.448
"65mil"	22.5	1.651	4.3335 (FR)	2.2268 (FR)	1.383
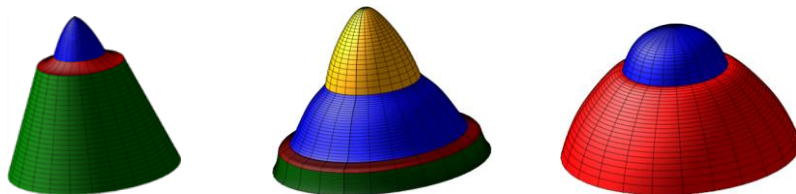
Figure 7: Averaged roughness element shapes defined by Finson [18], from left to right side, "11mil", "37mil" and "65mil" cases.

4.2 Comparison between experiment data and simulations

Simulations are performed with the N-S code and the boundary layer code CLICET. For this, boundary layer edge quantities are extracted from the N-S simulations using a criterium of 99.5 to 99.8 % of the freestream total enthalpy. Unfortunately, they are not so many detailed results presented in the original Hill's paper. Figure 8 presents the boundary layer velocity profile for the smooth wall and the *65mil* rough wall case. N-S simulations reproduce correctly the experiment data for both cases. In Figure 9, Stanton number from Finson's paper [17] are compared with N-S simulations. The Stanton number is evaluated using the boundary layer outer edge quantities:

$$S_t = \frac{\phi_w}{\rho_e u_e C_p (T_r - T_w)}$$

Simulations match well with experiment data in the case of smooth wall and rough wall with weak equivalent sand grain height (*11mil* case with Dirling correlation). For higher k_s values, corresponding to transient and fully rough regimes, a difference is noticeable between simulations and experiment data, including the *65mil* case for which velocities profile*s* are comparable. Simulations give overestimated values of the Stanton number (40% to 70%). N-S results are then compared to CLICET simulations showing a good agreement in wall heat flux evaluations for all the roughness patterns. The maximal difference observed on heat flux is of 5% for the *37mil* and *65mil* cases while it reaches 9% for the *11mil* case with W-K correlation. Figures 10, 11 and 12 show the resulting heat flux respectively for in *65mil, 11mil* and *37mil* cases. To interpret these discrepancies in the Stanton values, several potential origins can be pointed out: first, the application of the Stanton formulae is based on the boundary layer outer edge quantities which are extracted from N-S simulations. However, smooth wall Stanton numbers are well reproduced by simulations. Even accounting for the fact that slight modifications in N-S simulations could be found between smooth and rough cases, the uncertainty on outer edge quantity evaluation may not be sufficient to explain such discrepancies as observed in Figure 9 for the *37mil* and *65mil* cases. Another point is related to uncertainties coming from the use of averaged roughness shapes instead of real surface patterns and the application of correlations to evaluate k_s. The k_s value needed to retrieve the Stanton data level is of order of 5×10^{-4} m for the *65mil* case. However, it seems inconsistent with the reasonable agreement found for boundary layer velocity profiles shown in Figure 8. Averaged roughness elements are also used in the S_{corr} evaluation needed for thermal corrections. In this experiment configuration, wall roughness and thermal combined effects are expected to play an important role in the final heat flux level, according to the Reynolds analogy failure. It is worth noticing that in simulations, a weak 5% to 10% difference was found applying dynamic corrections only or both dynamic and thermal corrections. Heat flux sensitivity to the S_{corr} value was also noticed and could explain some difference with experiment data: this is under study. These simulations of Hill's experiments constitute a first step of the validation of Aupoix's k-ω SST corrections applied to hypersonic flows. While dynamic corrections provided reasonable results on velocity profiles, a deeper investigation is needed in the application of the thermal corrections to high Mach flows. This validation is still being pursued on the base of additional experiment data.
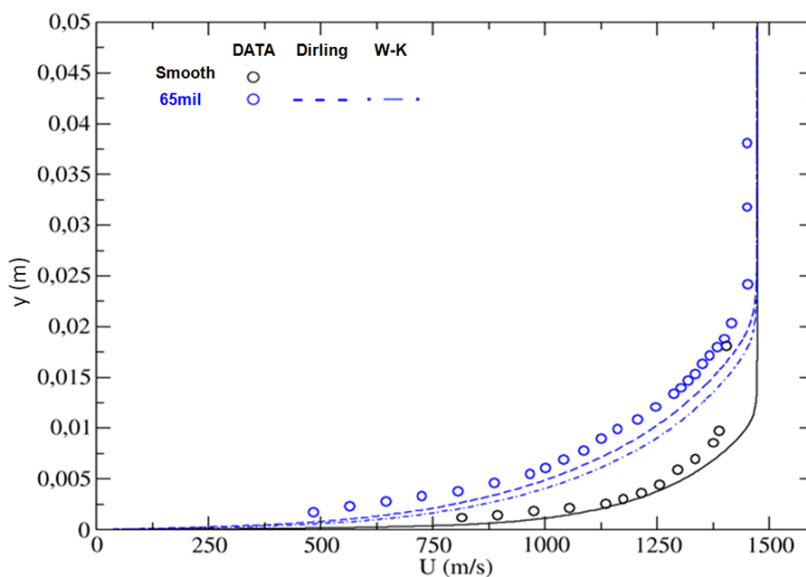
Figure 8: Boundary layer velocity profiles, experiment data (dots) from Hill's paper [17] and N-S simulations (plain) for smooth wall and *65mil* rough wall case
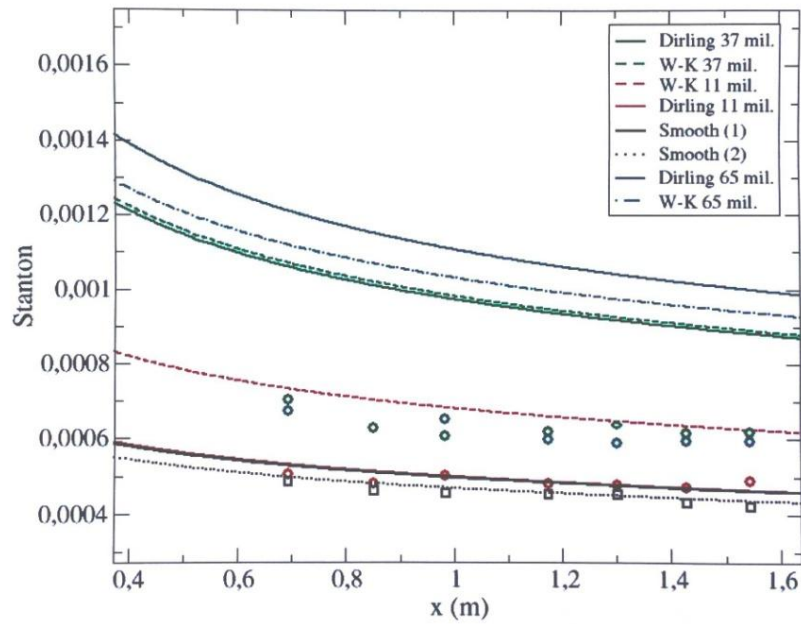
Figure 9: Stanton number obtained with N-S simulations and experiment data (dots/squares) given in ref. [18]
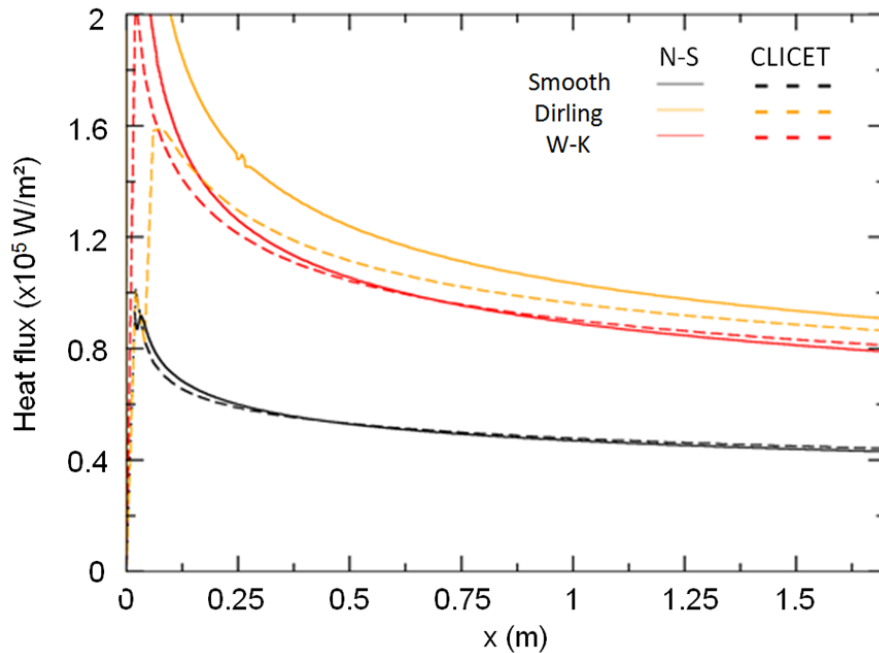
Figure 10: N-S and CLICET simulations - Heat flux at the wall for the *65mil* case

M. Olazabal-Loumé, F. Danvin, J. Mathiaud, B. Aupoix
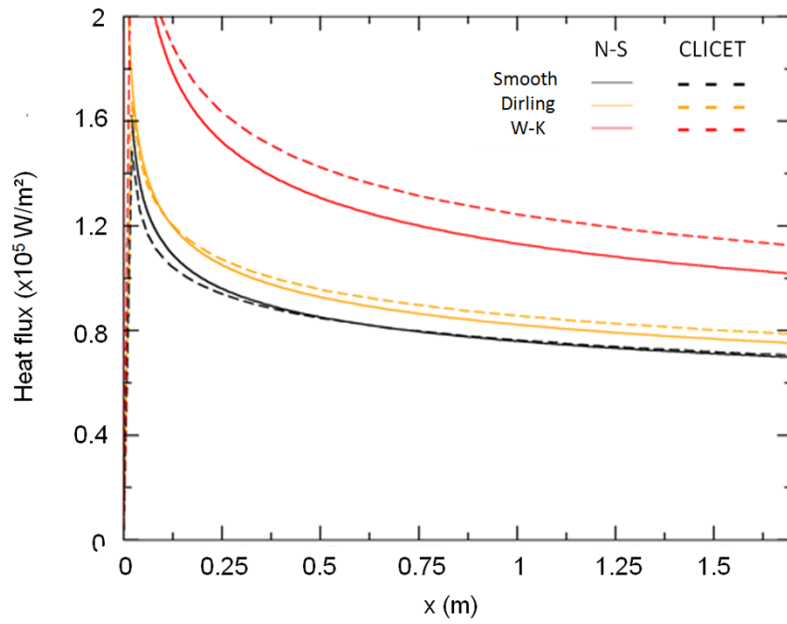
Figure 11: N-S and CLICET simulations - Heat flux at the wall for the *11mil* case
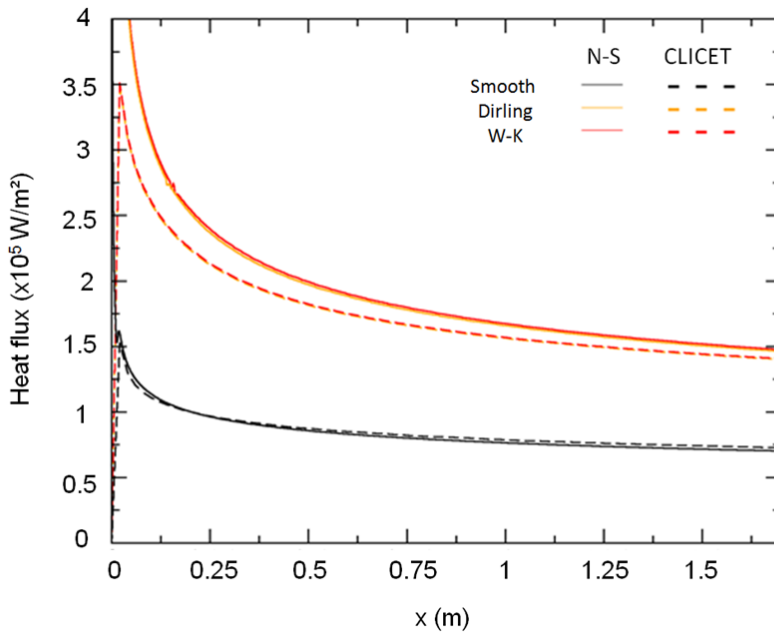
Figure 12: N-S and CLICET simulations - Heat flux at the wall for the *37mil* case

References

[1] Menter F. R. 1994. Two-equation eddy-viscosity turbulence models for engineering applications. AIAA journal. 32(8) :1598–1605.

[2] Aupoix B. 2015. Roughness corrections for the k–ω shear stress transport model : Status and proposals. Journal of Fluids Engineering. 137(2):021202.

[3] Aupoix B. 2015 Improved heat transfer predictions on rough surfaces. International Journal of Heat and Fluid flow.56:160-170

[4] Nikuradse J. 1933. Strömungsgesetze in rauhen rohren. Technical report, 361,VDI Forshungsheft, July/August.

[5] Nikuradse J. 1937. Laws of flows in rough pipes. Technical memorandum 1292, NACA, Washington, April.

[6] Schlichting H. 1936. Experimentelle untersuchungen zum rauhigkeitsproblem. Technical report, February.

[7] Schlichting H. 1937. Experimental investigation of the problem of surface roughness. Technical memorandum 823, NACA,Washington, April.

[8] Cousteix J. 1989. Turbulence et couche limite. Editions Cepadues.

[9] Grigson C. 1992. Drag losses of new ships caused by hull finish. Journal of Ship Research. 36(2):182–196.

[10] Colebrook C. and C. White. 1937. Experiments with fluid friction in roughened pipes. Proceedings of the Royal Society of London 161:367–381.

[11] Colebrook C. 1938–1939. Turbulent flow in pipes, with particular reference to the transition region between the smooth and rough pipe laws. Journal of Institution of Civil Engineering 21:133–156.

[12] Aupoix B. 2007. A general strategy to extend turbulence models to rough surfaces: Application to Smith's k-L model. Journal of fluids Engeneering, 129:1245.

[13] Wilcox D. C. 2010. Turbulence Modeling for CFD. Third Edition. DCW Industries.

[14] McClain S. T., S. P. Collins, B. K. Hodge, and J. P. Bons. 2006. The importance of the mean elevation in predicting skin friction for flow over closely packed surface roughness. Journal of Fluids Engineering, 128(3): 579–586.

[15] Aupoix B. 2010. Couches limites bidimensionnelles compressibles. descriptif et mode d'emploi du code CLICET – version 2010. Technical report. RT 1/117015 DMAE. ONERA.

[16] Roy C.J. and F.G. Blottner. 2006. Review and assessment of turbulence models for hypersonic flows, Progress in Aerospace Sciences, 42(7): 469–530.

[17] J.A.F. Hill, R.L.P. Voisinet, and D.A. Wagner. 1980. Measurements of surface roughness effects on the heat transfer to slender cones at mach 10. In American Institute of Aeronautics and Astronautics 18th Aerospace Sciences Meeting, Pasadena, California AIAA80-0345.

[18] Finson M.L. 1982. Study of turbulent boundary layer over rough surfaces, with emphasis on the effects of roughness character and Mach number. Technical Report ADA 1142217, Physical Sciences Inc. February.

[19] Dirling R.B. 1973. A method for computing rough wall heat transfer rates on reentry nose tips. AIAA paper 73-763. AIAA 8th Thermophysics Conference, Palm Springs, California, July 16-18.

[20] Waigh D.R. and R.J. Kind. 1998. Improved aerodynamic characterization of regular three dimensional Roughness. AIAA journal, 36(6) :1117–1119.